A Local Meshless Shepard and Least Square Interpolation Method Based on Local Weak Form

Y.C. Cai[1] and H.H. Zhu[1]

Abstract: The popular Shepard PU approximations are easy to construct and have many advantages, but they have several limitations, such as the difficulties in handling essential boundary conditions and the known problem of linear dependence regarding PU-based methods, and they are not the good choice for MLPG method. With the objective of alleviating the drawbacks of Shepared PU approximations, a new meshless PU-based Shepard and Least Square (SLS) interpolation is employed here to develop a new type of MLPG method, which is named as Local Meshless Shepard and Least Square (LMSLS) method. The SLS interpolation possesses the much desired Kronecker-delta property, hence the prescribed nodal displacement boundary conditions can be implemented as easily as in FEM. Based on the local Petrov-Galerkin weak form, the present LMSLS method utilizes a local polygonal domain to simplify the integration and the discrete equations and is a *truly* meshless method which constructs interpolation without using mesh and integrates the local weak form without a background mesh. Additionally, the orthogonal basis functions are used to totally eliminate the matrix inversion and matrix multiplication in the computation of the SLS interpolation. Numerical examples show that the present method has a high accuracy and convergence rate.

Keyword: Meshless, MLPG, point interpolation, Kronecker property, partition of unity.

1 Introduction

In recent years, a type of Meshless Local Petrov-Galerkin (MLPG) methods proposed by Atluri and Zhu (1998, 2000) has gained much attention in the area of meshless methods. The MLPG methods are truly meshless methods as no meshes are required either for the purposes of interpolation of the trial and test functions

[1] Key Laboratory of Geotechnical and Underground Engineering of Ministry of Education, Department of Geotechnical Engineering, School of Civil Engineering, Tongji University, 200092, P.R.China

or for the purposes of integration of the weak form. Various nodal-based meshless interpolation schemes, such as Moving Least Square (MLS) interpolation [Atluri and Zhu (2000)], Point Interpolation (PI) [Liu (2001)], Kriging Interpolation (KI) [Gu, Wang and Lam (2007)] and Radial Basis Function (RBF) [Gilhooley, Xiao and Batra (2008)] have been applied to a series of MLPG-type methods, and remarkable successes have been reported [Atluri and Shen (2005); Atluri, Liu and Han (2006a,2006b); Pecher, Elston and Raynes (2006); Vavourakis, Sellountos and Polyzos (2006); Atluri, Liu and Han (2006); Yuan, Chen and Liu (2007); Ma (2008)] . The MLPG methods have now been widely extended to a variety of problems including plate analysis [Sladek, Sladek, Wen and Aliabadi (2006); Sladek, Sladek, Krivacek, Wen and Zhang (2007); Jarak, Soric and Hoster (2007); Sladek, Sladek, Solek, Wen and Atluri (2008)], fracture mechanics [Gao, Liu and Liu (2006); Sladek, Sladek, Zhang, Solek and Starek (2007); Long, Liu and Li (2008)], 3D elasticity [Han and Atluri (2004)], topology-optimization of structures [Li and Atluri (2008a,2008b)], fluid flows [Arefmanesh, Najafi and Abdi (2008); Mohammadi (2008)], thermoanalysis [Ching and Chen (2006); Sladek, Sladek, Zhang and Tan (2006); Wu, Shen and Tao (2007); Sladek, Sladek, Zhang and Solek (2007)], dynamic analysis [Han, Liu, Rajendran and Atluri (2006); Ma (2007)], and others [Johnson and Owen (2007); Chen, Liu and Cen (2008); Dang and Sankar (2008)].

Generally, the MLPG method can also be based on the so-called Partition of Unity (PU). Partition of unity is a powerful tool in mathematics and has been widely used to constructed meshless approximations in the past decades. The PU-based approximations have many advantages including the freedom of selecting diverse local approximation spaces, the ability to enable the extrinsic basis to vary from node to node and thus facilitating *hp*-adaptivity, and the good tolerance to the distorted nodes. However, the popular PU functions [Babuška, Banerjee and Osborn (2004); Belytschko, Krongauz and Organ (1996); Griebel and Schweitzer (2002); Melenk and Babuška (1996); Oden, Duarte and Zienkiewicz (1998)] have several limitations such as the large increase of the unknowns at nodes when higher order polynomials are used, the difficulties in handling essential boundary conditions and the known problem of linear dependence regarding PU-based methods. Thus, as stated in Atluri and Shen (2002), the PU methods are not a good choice for MLPG method because the test functions also need more unknowns per node, otherwise sufficient equations cannot be obtained to determine the unknowns.

With the objective of alleviating the drawbacks and inheriting the advantages of the PU-based approximations, a new Local Meshless Shepard and Least Square (LMSLS) method based on the local Petrov-Galerkin weak form is proposed. The method employs the meshless Shepard and Least Square (SLS) interpolation proposed by the present authors as the trial function. The SLS interpolation is con-

structed by using the least-square shape function as a local approximation, and by using the Shepard shape function as a partition of unity. The SLS interpolation is truly meshless and possesses the *Kronecker-delta* property. The previously-mentioned disadvantages in the popular PU functions can be overcome, and the new PU-based SLS interpolation is well suited for developing a new type of MLPG method. Additionally, a new integration scheme over the sub-domain is proposed to simplify the integration and the discrete equations of the LMSLS method.

In order to simplify the computation of the SLS interpolation and avoid the ill-conditioned matrix in least square formulation, orthogonal basis functions are constructed for the SLS interpolation by using a Schmidt orthogonalization. The matrix inversion and matrix multiplication in the computation of the SLS interpolation can be totally eliminated through the use of the orthogonal basis functions.

The proposed LMSLS method is a *truly* meshless method which constructs interpolation without using mesh and integrates the local weak form without a background mesh. As far as we know this is also the first work of the local-weak form method using the PU-based approximation. Numerical results demonstrate the performance of the present method.

2 PU-based SLS interpolation

2.1 Popular Shepard PU approximations

If a domain Ω is covered by overlapping patches or sub- domains Ω^i, a general construction of PU approximation can be expressed as

$$u^h(\mathbf{x}) = \sum_i \chi_i(\mathbf{x}) L_i(\mathbf{x}) \tag{1}$$

where $L_i(\mathbf{x})$ are the polynomials of function centered about the node $\mathbf{x}_i$; The shape function $\chi_i(\mathbf{x})$ satisfies the zeroth order consistency condition.

Most of the meshless PU approximations [Babuška, Banerjee and Osborn (2004); Belytschko, Krongauz and Organ (1996); Griebel and Schweitzer (2002); Melenk and Babuška (1996); Oden, Duarte and Zienkiewicz (1998)] make use of the Shepard function as the partition of unity and choose polynomials as the local approximations. If we choose $L_i(\mathbf{x})$ to be:

$$L_i(\mathbf{x}) = \sum_J \beta_{Ji} p_J(\mathbf{x}) \tag{2}$$

where β_{Ji} are unknowns relevant to node i, $\mathbf{p}^T(\mathbf{x}) = [1, x, y, \cdots]$ are polynomial basis functions. The Shepard PU approximations can be written as

$$u^h(\mathbf{x}) = \sum_i \phi_i^0(\mathbf{x}) \sum_J \beta_{Ji} p_J(\mathbf{x}) \tag{3}$$

where

$$\phi_i^0(\mathbf{x}) = \frac{w_i(\mathbf{x})}{\sum\limits_{j=1}^{n} w_j(\mathbf{x})} \tag{4}$$

is the known Shepard function or the zeroth-order MLS shape function, $w_i(\mathbf{x})$ is the weight function associated with node i, n is the number of nodes such that $w_i(\mathbf{x}) > 0$.

By introducing higher order polynomials $L_i(\mathbf{x})$ in Eq.(3), the performance of the PU approximation can be improved. For example, if we use linear basis $p_J(\mathbf{x})$, the Shepard PU approximation in Eq.(3) can attain linear consistency. The Shepard PU approximations are easy to construct and have many advantages. Nevertheless, note that this kind of method requires at least three unknowns per node in a 2-dimensional problem in order to attain linear consistency. This may lead to singular global matrices due to the known problem of linear dependence regarding PU based methods and may bring difficulties to the imposition of the essential boundary conditions. Furthermore, as stated in Atluri and Shen (2002), PU methods are not a good choice for the MLPG method because the test functions also need more unknowns per node to obtain sufficient equations to determine unknowns.

Several other PU-constructions in the literature [Macri and De (2008); Oh, Kimb and Honga (2008); Rajendran and Zhang (2007)] are proposed to partially overcome the drawbacks of the PU methods. However, the requirement of a FE mesh is a demerit in these PU methods as compared to meshfree methods.

2.2 PU-based SLS interpolation

Here a PU-based meshless Shepard and Least Square (SLS) interpolation is employed wherein the Shepard shape function is used for partition of unity, and the least square shape function is used for local approximation. By using this kind of SLS interpolation, most problems of the popular Shepard PU approximations can be eliminated.

Suppose that the support of node i is defined by a circle of radius d_{mi} with $\mathbf{x}_i$ as its centre, and there are M nodes in the support Ω^i (Fig.1). For a given point $\mathbf{x}\,(\mathbf{x} \in \Omega)$, the SLS interpolation $u^h(\mathbf{x})$ at $\mathbf{x}$ can be defined by

$$u^h(\mathbf{x}) = \sum_{i=1}^{n} \phi_i^0(\mathbf{x}) u^{Li}(\mathbf{x}) \tag{5}$$

where the local approximation $u^{Li}(\mathbf{x})$ is defined as

$$u^{Li}(\mathbf{x}) = \sum_{J=1}^{M} \Phi_J^i(\mathbf{x}) u_J \tag{6a}$$

and

$$\Phi_J^i(\mathbf{x}) = \sum_{j=1}^{m} p_j(\mathbf{x}) \left(\mathbf{A}^{-1}\mathbf{B}\right)_{jJ} \tag{6b}$$

is the least square function associated with node $J\,(J=1,\cdots,M)$; m is the number of terms in the basis; and

$$\mathbf{B} = \mathbf{P}^T = \begin{bmatrix} \mathbf{p}(\mathbf{x}_1) & \mathbf{p}(\mathbf{x}_2) & \cdots & \mathbf{p}(\mathbf{x}_M) \end{bmatrix} \tag{6c}$$

$$\mathbf{A} = \mathbf{P}^T\mathbf{P} \tag{6d}$$
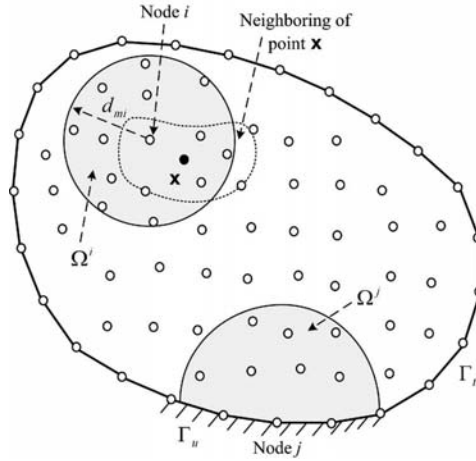
Figure 1: Discrete model of domain Ω

The least-square approximation in Eq.(6) does not satisfy the condition of $u^{Li}(\mathbf{x}_i) = u_i$ at node i and will bring difficulties in the imposition of essential boundary conditions. Therefore, we make a modification to Eq.(6) as

$$u^{Li}(\mathbf{x}) = \sum_{J=1}^{M} \bar{\Phi}_J^i(\mathbf{x})u_J = \bar{\Phi}^i\mathbf{u} \tag{7a}$$

where

$$\bar{\Phi}^i(\mathbf{x}) = \left[\Phi_1^i(\mathbf{x}) - \Phi_1^i(\mathbf{x}_i), \cdots, 1 + \Phi_i^i(\mathbf{x}) - \Phi_i^i(\mathbf{x}_i), \cdots, \Phi_M^i(\mathbf{x}) - \Phi_M^i(\mathbf{x}_i)\right] \tag{7b}$$

$$\mathbf{u}^T = [u_1, u_2, \cdots, u_M] \tag{7c}$$

and $\mathbf{x}_i$ is the coordinate of node i.

From Eq.(7b) we can obtain $\bar{\Phi}_i^i(\mathbf{x}_i) = 1$ and $\bar{\Phi}_J^i(\mathbf{x}_i) = 0$ $(J \neq i)$ at $\mathbf{x} = \mathbf{x}_i$, and $\sum_{J=1}^{M} \bar{\Phi}_J^i(\mathbf{x}) = 1$. This means that $u^{Li}(\mathbf{x}_i) = u_i$ is satisfied in the modified Eq.(7).

Substituting Eq.(7) into Eq.(5) leads to the following formulation of a new meshless point interpolation approximation:

$$u^h(\mathbf{x}) = \sum_{i=1}^{n} \phi_i^0(\mathbf{x}) u^{Li}(\mathbf{x}) = \sum_{i=1}^{n} \phi_i^0(\mathbf{x}) \left(\sum_{J=1}^{M} \bar{\Phi}_J^i(\mathbf{x}) u_J \right) \tag{8}$$

Let R be the total number of nodes, which are in the supports of all the nodes associated with the given point $\mathbf{x}$ such that $w_i(\mathbf{x}) > 0, (i = 1, 2, \cdots, n)$. Eq.(8) can be rewritten as

$$u^h(\mathbf{x}) = \begin{Bmatrix} \phi_1^0 \\ \phi_2^0 \\ \vdots \\ \phi_n^0 \end{Bmatrix}^T \begin{bmatrix} \bar{\Phi}_1^1 & \cdots & \bar{\Phi}_n^1 & \bar{\Phi}_{n+1}^1 & \cdots & \bar{\Phi}_R^1 \\ \bar{\Phi}_1^2 & \cdots & \bar{\Phi}_n^2 & \bar{\Phi}_{n+1}^2 & \cdots & \bar{\Phi}_R^2 \\ \vdots & \cdots & \vdots & \vdots & \cdots & \vdots \\ \bar{\Phi}_1^n & \cdots & \bar{\Phi}_n^n & \bar{\Phi}_{n+1}^n & \cdots & \bar{\Phi}_R^n \end{bmatrix} \begin{Bmatrix} u_1 \\ u_2 \\ \vdots \\ u_R \end{Bmatrix}$$

$$= \mathbf{\Phi}^0_{1 \times n} \bar{\mathbf{\Phi}}_{n \times R} \mathbf{u}_{R \times 1} = \sum_{k=1}^{R} \bar{N}_k(\mathbf{x}) u_k \tag{9}$$

where $\mathbf{\Phi}^0$ is the vector of the Shepard shape function associated with the n neighboring nodes of the given point $\mathbf{x}$, $\bar{\mathbf{\Phi}}$ is the matrix of the modified Least Square Point Interpolation(LSPI) shape function, and $\bar{N}_k(\mathbf{x})$ is the SLS shape used later in this paper.

The commonly used bases in Eq.(6) in 2-D problems are the linear basis:

$$\mathbf{p}^T(\mathbf{x}) = [1, x, y] \tag{10a}$$

or the quadratic basis:

$$\mathbf{p}^T(\mathbf{x}) = \left[1, x, y, xy, x^2, y^2\right] \tag{10b}$$

The linear dependence problem has been a bottleneck for the PU-based method in which both the PU functions and the local functions are taken as explicit polynomials. However, the present SLS interpolation naturally eliminates the linear dependency problem associated with other PU-based approximations because no additional degrees of freedom have been added to the global stiffness matrix and the definition of the local approximations as shown in Eq.(9). Also, the limitation

of the PU-based approximation in the application of the local weak form can be overcome.

Krongauz and Belytschko (1997) proposed another meshless method satisfying the linear consistency by using the Shepard function, but this method is applicable to the limited problems only when the derivatives of an unknown function appear in a PDE.

2.3 *Weight functions of the SLS interpolation*

The Shepard function $\phi_i^0(\mathbf{x})$ in Eq.(4) satisfies the *Kronecker-delta* property if weight function $w_i(\mathbf{x})$ is singular at $\mathbf{x} = \mathbf{x}_i$. The following singular weight function [Lancaster and Salkauskas (1981)] is used in this study:

$$
w_i(\mathbf{x}) = \begin{cases} \frac{d_{mi}^2}{d_i^2 + \varepsilon} \cos^2\left(\frac{\pi d_i}{2d_{mi}}\right), & d_i \le d_{mi} \\ 0, & d_i > d_{mi} \end{cases}
\tag{11}
$$

where d_{mi} is the radius of support of node i; $d_i = \|\mathbf{x} - \mathbf{x}_i\|$ is the Euclidian distance between point $\mathbf{x}$ and node $\mathbf{x}_i$; and $\varepsilon = 1\mathrm{E} - 10$ is a small number to avoid the numerical difficulty resulting from the singularity at nodes.

The support d_{mi} for node i(Figure 1) is taken as

$$
d_{mi} = \alpha \cdot b \cdot c_i
\tag{12}
$$

where α is a coefficient chosen as $1.1 \le \alpha \le 3.5$; b is a coefficient in which $b = 2$ is for the nodes at the boundary, and $b = 1$ is for the other nodes; and c_i is chosen as the distance to the fourth nearest neighbor of node i.

2.4 *Properties of the SLS interpolation*

2.4.1 *Kronecker-delta property of $\bar{N}_k(\mathbf{x})$*

At the n neighboring nodes of the given point $\mathbf{x}$, the shape function $\bar{N}_k(\mathbf{x})$ of the SLS satisfies the following *delta* property because of the properties of $\bar{\Phi}_i^i(\mathbf{x}_i) = 1$ and $\bar{\Phi}_k^i(\mathbf{x}_i) = 0\,(k \ne i)$ in Eq.(7b), and $\phi_k^0(\mathbf{x}_i) = \delta_{ik}$ in Eq.(9):

$$
\bar{N}_k(\mathbf{x}_i) = \delta_{ki}, (i = 1, 2, \cdots, n)
\tag{13}
$$

If we evaluate Eq.(9) at an arbitrary node i, i.e. at $\mathbf{x} = \mathbf{x}_1$, we obtain

$$
\bar{\mathbf{N}}(\mathbf{x}_1) = \left\{\begin{matrix} 1 \\ 0 \\ \vdots \\ 0 \end{matrix}\right\}^T \left[\begin{array}{cccc|ccc} 1 & 0 & \cdots & 0 & 0 & \cdots & 0 \\ \bar{\Phi}_1^2(\mathbf{x}_1) & \bar{\Phi}_2^2(\mathbf{x}_1) & \cdots & \bar{\Phi}_n^2(\mathbf{x}_1) & \bar{\Phi}_{n+1}^2(\mathbf{x}_1) & \cdots & \bar{\Phi}_R^2(\mathbf{x}_1) \\ \vdots & \vdots & \cdots & \vdots & \vdots & \cdots & \vdots \\ \bar{\Phi}_1^n(\mathbf{x}_1) & \bar{\Phi}_2^n(\mathbf{x}_1) & \cdots & \bar{\Phi}_n^n(\mathbf{x}_1) & \bar{\Phi}_{n+1}^n(\mathbf{x}_1) & \cdots & \bar{\Phi}_R^n(\mathbf{x}_1) \end{array}\right]
$$

$$
= \left\{\begin{matrix} 1 \\ 0 \\ \vdots \\ 0 \end{matrix}\right\}
\tag{14}
$$

and

$$
u^h(\mathbf{x}_1) = \sum_{k=1}^R \bar{N}_k(\mathbf{x}_1) u_k = u_1
\tag{15}
$$

Similarly we can show that

$$
u^h(\mathbf{x}_2) = \sum_{k=1}^R \bar{N}_k(\mathbf{x}_2) u_k = u_2
$$

$$
\cdots\cdots
\tag{16}
$$

$$
u^h(\mathbf{x}_n) = \sum_{k=1}^R \bar{N}_k(\mathbf{x}_n) u_k = u_n
$$

Thus, the shape function $\bar{N}_k(\mathbf{x})$ possesses the desirable delta property and hence the nodal displacement boundary conditions in the present work can be imposed as easily as in FEM.

2.4.2 Completeness property

The Shepard function $\phi_i^0(\mathbf{x})$ in Eq.(4) is the lowest order form of MLS shape functions. It has zeroth-order completeness because it only reproduces const functions exactly, which leads to poor results for solving elastostatics. In contrast, the SLS interpolation in Eq.(9) is capable of exactly reproducing any function which appears in the basis of $\mathbf{p}(\mathbf{x})$ in Eq.(10). The proof is given below:

Consider any arbitrary displacement field given by

$$
\tilde{u}(x,y) = b_1 + b_2 x + b_3 y + b_4 xy + \cdots
\tag{17}
$$

Substituting Eq.(17) into Eq.(7) results in

$$
\begin{aligned}
u^{Li}(\mathbf{x}) &= \sum_{J=1}^{M} \bar{\Phi}_J^i(\mathbf{x})\tilde{u}(\mathbf{x}_J) \\
&= \sum_{J=1}^{M} \Phi_J^i(\mathbf{x})\tilde{u}(\mathbf{x}_J) - \sum_{J=1}^{M} \Phi_J^i(\mathbf{x}_i)\tilde{u}(\mathbf{x}_J) + \tilde{u}(\mathbf{x}_i)
\end{aligned}
\tag{18}
$$

Since any function in the basis can be reproduced exactly in the least square approximation, it follows that

$$
\tilde{u}(\mathbf{x}) = \sum_{J=1}^{M} \Phi_J^i(\mathbf{x})\tilde{u}(\mathbf{x}_J)
\tag{19}
$$

Using Eq.(19) in Eq.(18) leads to

$$
u^{Li}(\mathbf{x}) = \tilde{u}(\mathbf{x}) - \tilde{u}(\mathbf{x}_i) + \tilde{u}(\mathbf{x}_i) = \tilde{u}(\mathbf{x})
\tag{20}
$$

Substituting Eq.(20) in Eq.(8) yields

$$
u^h(\mathbf{x}) = \sum_{i=1}^{n} \phi_i^0(\mathbf{x})u^{Li}(\mathbf{x}) = \tilde{u}(\mathbf{x}) \cdot \sum_{i=1}^{n} \phi_i^0(\mathbf{x}) = \tilde{u}(\mathbf{x})
\tag{21}
$$

Thus, the SLS interpolation preserves completeness up to the order of the basis.

2.4.3 *Comparison of LS, MLS and SLS approximations*

Least square approximation by polynomials is in widespread use, and is much simpler and more efficient for computation and derivation by comparison with the MLS approximation. The main drawback of the LS approach in Eq. (6) is that the approximation rapidly deteriorates if the number of points used largely exceeds that of the m polynomial terms in $\mathbf{p}(\mathbf{x})$. However, this deficiency can be overcome in the present Shepard Least-Square (SLS) interpolation.

The accuracy of the numerical solution will very much depend on the shape functions used in each approximation. To understand better the differences of the LS, MLS and SLS approximations, we plot some of the shape functions resulting from these methods in one dimension.

The weight function used in the MLS method is the same as in Belytschko, Lu and Gu (1994):

$$
w_i(\mathbf{x}) = \begin{cases} \dfrac{e^{-(d_i/c_i)^2} - e^{-(d_{mi}/c_i)^2}}{1 - e^{-(d_{mi}/c_i)^2}}, & \text{if } d_i \le d_{mi} \\ 0, & \text{if } d_i > d_{mi} \end{cases}
\tag{22}
$$
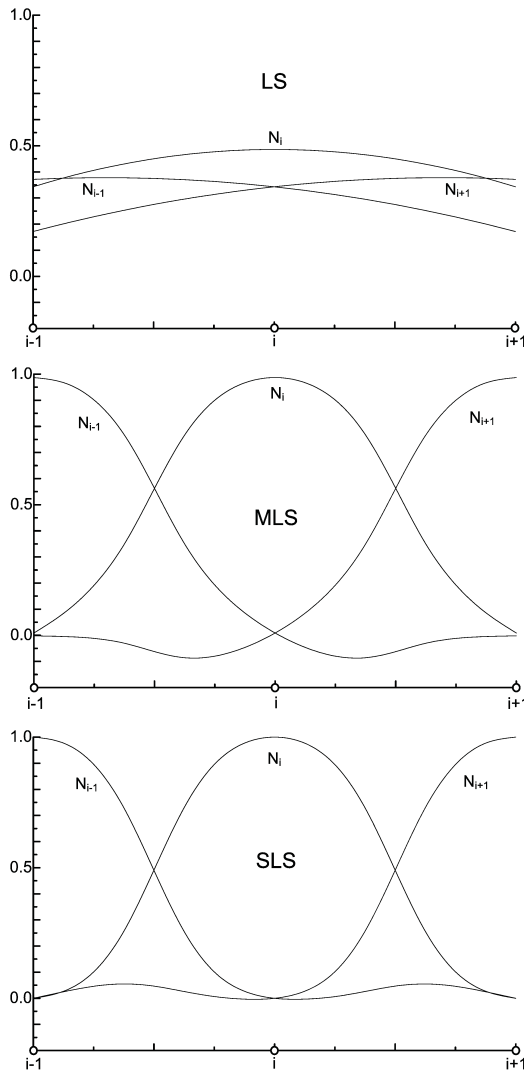
Figure 2: Shape functions $N_i(x)$ for $\mathbf{p} = (1, x, x^2)$

where d_{mi} is the nodal support decided by Eq.(12) and $c_i = 0.3d_{mi}$ is used in this paper.

Fig.2 shows the shape functions for a quadratic basis ($m = 3$). The node space is 1 and the nodal support is 2.5. Note that the LS method yields very inaccurate interpolating functions in this case with the value $N_i(x)$ less than 0.5 everywhere. The SLS interpolation gives $N_i(x) = 1$ at $x = x_i$ and $N_i(x) = 0$ at $x = x_j$, $j \neq i$.

2.5   *Orthogonal algorithm of the SLS interpolation*

The necessity for solving Eq.(6a) can be eliminated by diagonalizing the matrix **A**. For a given arbitrary basis function $p_k(\mathbf{x}) (k = 1, \cdots, m)$, the orthogonal basis function $q_k(\mathbf{x}) (k = 1, \cdots, m)$ is obtained by using the Schmidt orthogonalization procedure [Lu and Belytschko (1994)] as follows:

$$q_k(\mathbf{x}) = p_k(\mathbf{x}) - \sum_{j=1}^{k-1} \alpha_{kj} q_j(\mathbf{x}), \quad k = 1, \cdots, m \tag{23a}$$

where

$$\alpha_{kj} = \frac{\sum\limits_{I=1}^{M} p_k(\mathbf{x}_I) q_j(\mathbf{x}_I)}{\sum\limits_{I=1}^{M} q_j^2(\mathbf{x}_I)} \tag{23b}$$

Above orthogonal function $q_k(\mathbf{x})$ satisfies the following orthogonality condition

$$\sum_{I=1}^{M} q_k(\mathbf{x}_I) q_j(\mathbf{x}_I) = 0, \quad k \neq j \tag{24}$$

Because of the orthogonality condition (24), by using the orthogonal function $q_k(\mathbf{x})$ in the least square procedure, Eq.(6) is written as

$$u^{Li}(\mathbf{x}) = \sum_{J=1}^{M} \Phi_J^i(\mathbf{x}) u_J \tag{25a}$$

where the shape function $\Phi_J^i(\mathbf{x})$ is defined by

$$\Phi_J^i(\mathbf{x}) = \sum_{k=1}^{m} q_k(\mathbf{x}) C_{kJ}(\mathbf{x}_J) \tag{25b}$$

$$C_{kJ}(\mathbf{x}_J) = \frac{q_k(\mathbf{x}_J)}{\sum\limits_{J=1}^{M} q_k^2(\mathbf{x}_J)} \tag{25c}$$

The derivatives of $\Phi_J^i(\mathbf{x})$ can be obtained as

$$\Phi_{J,l}^i(\mathbf{x}) = \sum_{k=1}^{m} q_{k,l}(\mathbf{x}) C_{kJ}(\mathbf{x}_J) \tag{26a}$$

where

$$q_{k,l}(\mathbf{x}) = p_{k,l}(\mathbf{x}) - \sum_{j=1}^{k-1} \alpha_{kj} q_{j,l}(\mathbf{x}), \quad k = 1, \cdots, m \tag{26b}$$

The PU-based SLS shape function may be looked upon as a composite function of Shepard and least square shape functions. The composite SLS shape function possesses the strengths of MLS and PU methods and at the same time overcome the major drawbacks of these methods. The following are the prominent merits of the SLS interpolation:

The SLS shape function is free from the linear dependence problem which is known in PU-based method and possesses the much desired Kronecker-delta property.

The SLS interpolation is capable of exactly reproducing any function which appears in the basis.

The proposed method inherits the advantages of PU-based method wherein high order global approximation can be obtained by simply increasing the order of the local approximation without necessarily adding new nodes.

The burden of matrix inversion and matrix multiplication in the SLS interpolation can be totally eliminated, and the problem of ill-conditioned matrix of the least-square method can be solved.

From Eq.(25) and Eq.(26) we can find that both the computation and the derivation of the present SLS interpolation are much simpler than that of the MLS approximation.

Although the SLS shape functions possess the Kronecker-delta property and hence the facility to impose the prescribed nodal displacement boundary conditions, the satisfaction of exact displacement boundary conditions all along the edges is not guaranteed by simply enforcing the boundary conditions at the nodes. The penalty method or Lagrange multiplier method may have to be used for the purpose. This aspect is rather similar to other point interpolation meshless methods.

3   The local weak form of LMSLS

For domain Ω bounded by Γ (Fig.3), the equilibrium equations and boundary conditions of linear elasticity are given by

$$\begin{cases} \sigma_{ij,j} + b_i = 0 & \text{in } \Omega \\ u_i = \bar{u}_i & \text{at } \Gamma_u \\ \sigma_{ij} n_j = \bar{t}_i & \text{at } \Gamma_t \end{cases} \tag{27}$$

where σ_{ij} is the stress tensor, b_i are the body forces, n_j are the unit normal to the domain, Γ_u and Γ_t are the global boundaries with prescribed displacements and tractions, respectively.
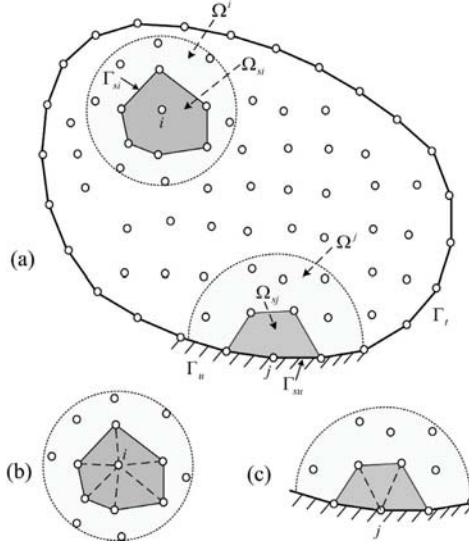
Figure 3: (a) The support and integration domains;(b)The construction of the local integral domain for an interior node; (c) The construction of the local integral domain for a boundary node

A generalized local weak form of the equilibrium equation is written as

$$\int_{\Omega_{si}} v_i \left(\sigma_{ij,j} + b_i \right) d\Omega = 0 \tag{28}$$

where Ω_{si} is the integration domain or sub-domain for node i, v_i is the test function. Using the divergence theorem in Eq.(28), we obtain the following local weak-form:

$$\int_{\partial\Omega_{si}} v_i \sigma_{ij} n_j d\Gamma - \int_{\Omega_{si}} \left(v_{i,j} \sigma_{ij} - v_i b_i \right) d\Omega = 0 \tag{29}$$

where n_j is the outward unit normal to the boundary $\partial\Omega_{si}$. The boundary $\partial\Omega_{si}$ for the sub-domain Ω_{si} is usually composed of three parts: the internal boundary Γ_{si}, the boundary Γ_{su} and Γ_{st}, over which the essential and natural boundary conditions are specified. Noticing that $\sigma_{ij} n_j = \bar{t}_i$ in Eq.(29), it is obtained that

$$\int_{\Gamma_{si}} v_i t_i d\Gamma + \int_{\Gamma_{su}} v_i t_i d\Gamma + \int_{\Gamma_{st}} v_i \bar{t}_i d\Gamma - \int_{\Omega_{si}} \left(v_{i,j} \sigma_{ij} - v_i b_i \right) d\Omega = 0 \tag{30}$$

Different interpolations can be used for the test and trail functions in the local weak form. Circular, elliptical, rectangular and others can be selected as the nodal sub-domains. Furthermore, the sizes and shapes of the sub-domains of the test and trial functions do not need to be the same. Depending upon the choice of test functions, six MLPG formulations [Atluri and Shen (2002)] known as MLPG1 through MLPG6 have been developed. Of course, the test functions in these MLPG methods can be chosen as the test function in the present LMSLS.

For the purpose of simplifying the integration and the discrete equations of LMSLS, the local polygonal sub-domains are constructed as the integration domains Ω_{si} in this paper.

Regarding the M nodes in the support of node i, a local polygon can be constructed based on Delaunay algorithm as shown in Fig.3(b) and Fig.3(c). Similar n-sided polygons or triangular domains are used to be the local domains in Barry (2004) and Cai and Zhu (2004). However, their implementations require the construction of global meshes, hence they lose the truly meshless character of the MLPG method. Here, the local polygon is redefined by the M nodes in the support of i, and it is obvious that the present LMSLS is truly meshless. Also, the construction of the local polygon is simple and efficient because the Delaunay algorithm is only performed in the support of node i.

In order to simplify the equation (30), we can deliberately select the test functions v_i such that they vanish over Γ_{si}. This can be easily accomplished by selecting the three-node triangular FEM shape functions N_i, which correspond to the node i of the triangles constructing the polygonal sub-domain Ω_{si}, as test functions v_i. Using shape functions N_i in equation (30), we obtain the following local weak form:

$$\int_{\Gamma_{su}} N_i t_i d\Gamma + \int_{\Gamma_{st}} N_i \bar{t}_i d\Gamma - \int_{\Omega_{Si}} (N_{i,j}\sigma_{ij} - N_i b_i)\, d\Omega = 0 \tag{31}$$

For a local polygonal sub-domain Ω_{si} located entirely with the global domain Ω, there is no intersection between $\partial\Omega_{si}$ and the global boundary Γ, and the integrals over Γ_{su} and Γ_{st} in equation (31) vanish.

Substituting the SLS approximation in Eq.(9) into the above equation leads to the following discretized system of linear equations:

$$\left(\int_{\Omega_{si}} \mathbf{v}_i^T \mathbf{DB}\, d\Omega - \int_{\Gamma_{su}} \mathbf{N}_i \mathbf{nDB}\, d\Gamma \right) \cdot \mathbf{U} = \int_{\Gamma_{st}} \mathbf{N}_i \bar{\mathbf{t}}\, d\Gamma + \int_{\Omega_{si}} \mathbf{N}_i \mathbf{b}\, d\Omega \tag{32}$$

recorded as

$$\mathbf{KU} = \mathbf{F} \tag{33a}$$

where $\mathbf{D}$ is the elasticity matrix, $\mathbf{n}$ is the matrix of the outward normal,

$$\mathbf{v}_i = \begin{bmatrix} N_{i,x} & 0 \\ 0 & N_{i,y} \\ N_{i,y} & N_{i,x} \end{bmatrix} \tag{33b}$$

$$\mathbf{N}_i = \begin{bmatrix} N_i & 0 \\ 0 & N_i \end{bmatrix} \tag{33c}$$

$$\mathbf{n} = \begin{bmatrix} n_1 & 0 & n_2 \\ 0 & n_2 & n_1 \end{bmatrix} \tag{33d}$$

$$\mathbf{B} = \begin{bmatrix} \bar{N}_{1,x} & 0 & \cdots & \bar{N}_{R,x} & 0 \\ 0 & \bar{N}_{1,y} & \cdots & 0 & \bar{N}_{R,y} \\ \bar{N}_{1,y} & \bar{N}_{1,x} & \cdots & \bar{N}_{R,y} & \bar{N}_{R,x} \end{bmatrix} \tag{33e}$$

$$\mathbf{U} = \left\{ u_1 \quad v_1 \quad \cdots \quad u_R \quad v_R \right\} \tag{33f}$$

Equation (33) can be individually integrated over each triangle constructing the local sub-domain Ω_{si}, as shown in Fig.3b and Fig.3c. In the present work, three Gaussian points are used in each triangle.

4   Numerical example

The proposed LMSLS is programmed in C++. A series of numerical examples are tested to study the efficiency of the present method. The results are compared with the exact solutions, the MLPG1 solutions using MLS shape functions and the results of reference solutions where available. In all examples, the MLPG1 method employs the same numerical integration as the LMSLS method.

4.1   Standard patch tests

The first example is the standard patch test. The three patches shown in Fig.4 are tested. In these patch tests, the displacements are prescribed on all outside boundaries by a linear function of x and y. Satisfaction of the patch test requires that the displacement of interior nodes be given by the same linear function, and the stress and strain be constant in the patch.

Since the exact solution is linear, a linear basis for the SLS interpolation is able to represent this solution. $\alpha = 1.1$ in Eq.(12) is used in this case. A linear elastic material with $E = 1$ and $v = 0.25$ is considered. The essential boundary conditions are imposed at the discrete boundary nodes directly. The computational results in Tab.1 show that the LMSLS passes the standard patch tests exactly.

(a) regular nodes   (b) irregular nodes

(c) irregular nodes
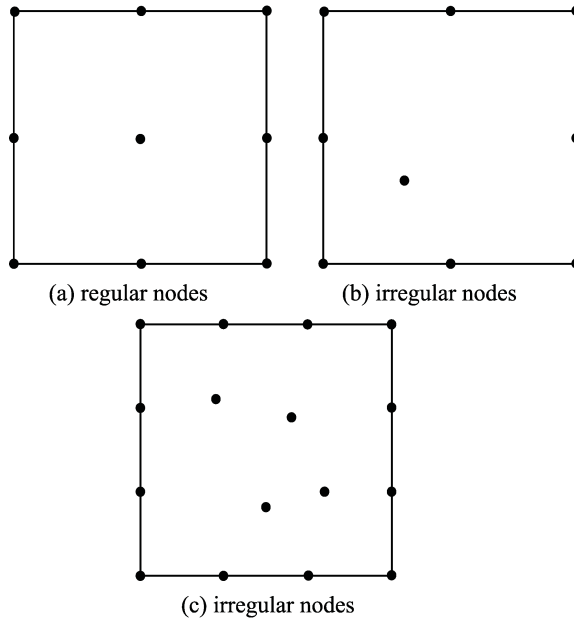
Figure 4: Nodal arrangements for the standard patch tests

Table 1: Computational results of the patch tests

Coordinates of interior nodes			Displacements		
Nodes (a)	Nodes (b)	Nodes (c)	Nodes (a)	Nodes (b)	Nodes (c)
1.0,1.0	0.8,0.9	1.0,2.0	1.0,1.0	0.8,0.9	1.0,2.0
-	-	1.5,0.8	-	-	1.5,0.8
-	-	1.9,1.8	-	-	1.9,1.8
-	-	2.1,0.9	-	-	2.1,0.9

4.2   A constant strain patch test

A constant strain patch test [Rajendran and Zhang (2007)] using three distributions of 7, 28 and 126 irregular nodes is shown in Fig.5. The Young's modulus is 1000, Poission's ration is 0.25 and the thickness of the plate is 1.

Since the exact solution is linear, a linear basis for the SLS interpolation is able to represent this solution. $\alpha = 1.1$ in Eq.(12) is used in this case. The computational results in Tab.2 show that the present LMSLS passes the patch tests exactly.
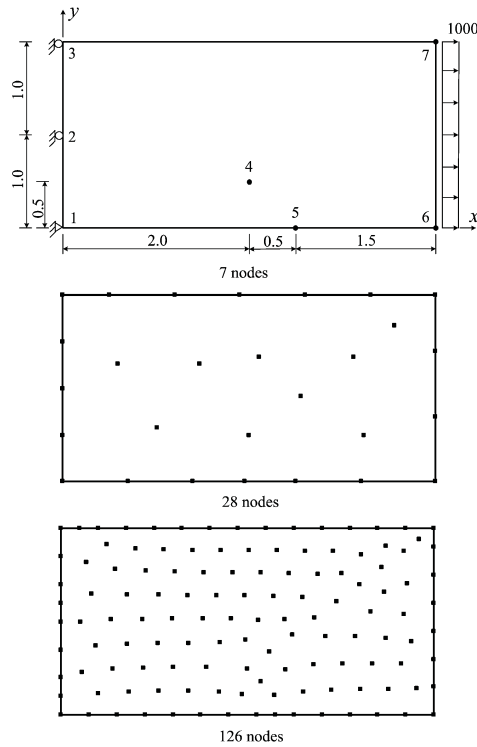
Figure 5: Nodal arrangements for the constant strain patch tests

Table 2: Results of the constant strain patch test

Number of nodes	u_4	v_4	u_5	v_5	u_7	v_7
7	2.0	-0.125	2.5	0.0	4.0	-0.5
28	2.0	-0.125	2.5	0.0	4.0	-0.5
126	2.0	-0.125	2.5	0.0	4.0	-0.5
Exact	2.0	-0.125	2.5	0.0	4.0	-0.5

4.3   Cantilever beam

Consider a cantilever beam of dimensions $l = 8m$ and $d = 1m$ subjected to a tip shear force at the free end as shown in Fig.6a. The material properties are $E = 1 \times 10^5 Pa$ and $v = 0.25$. The problem is solved for the plane stress case.

In order to study the convergence of LMSLS and to make error estimation, dis-

(a) Cantilever beam

(b) Nodal arrangement
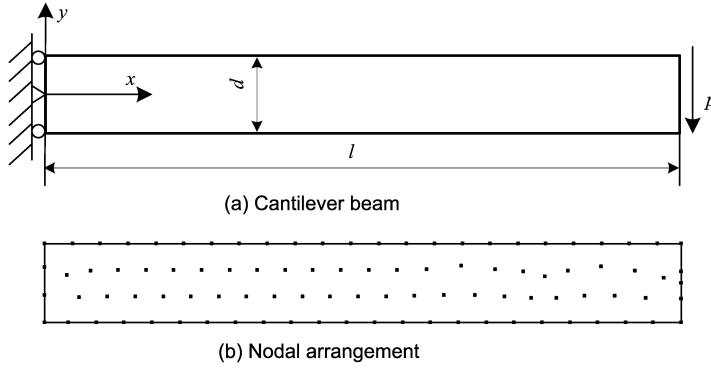
Figure 6: Cantilever beam and its nodal arrangement

placement norm and energy norm are defined by

$$\|\mathbf{u}\| = \left(\int_\Omega \mathbf{u}^T \cdot \mathbf{u} d\Omega \right)^{\frac{1}{2}}, \quad \|\boldsymbol{\varepsilon}\| = \left(\int_\Omega \boldsymbol{\varepsilon}^T \cdot \sigma d\Omega \right)^{\frac{1}{2}} \tag{34}$$

Relative error is defined by

$$r_u = \frac{\|\mathbf{u}^{num} - \mathbf{u}^{exact}\|}{\|\mathbf{u}^{exact}\|}, \quad r_e = \frac{\|\boldsymbol{\varepsilon}^{num} - \boldsymbol{\varepsilon}^{exact}\|}{\|\boldsymbol{\varepsilon}^{exact}\|} \tag{35}$$

The analytical solution to this problem is given by Timoshenko and Goodier (1970):

$$\sigma_x(x,y) = \frac{p(l-x)y}{I} \tag{36a}$$

$$\sigma_y = 0 \tag{36b}$$

$$\tau_{xy}(x,y) = -\frac{P}{2I}\left(\frac{d^2}{4} - y^2\right) \tag{36c}$$

$$u_x = -\frac{py}{6EI}\left[(6l-3x)x + (2+v)\left(y^2 - \frac{d^2}{4}\right)\right] \tag{36d}$$

$$u_y = -\frac{p}{6EI}\left[3vy^2(l-x) + (4+5v)\frac{d^2x}{4} + (3l-x)x^2\right] \tag{36e}$$

where $I = \frac{d^3}{12}$ is the second moment of area of the beam.

The quadratic basis function is used in this example. Four distributions of 50,138,486 and 965 nodes are employed respectively for the convergence studies. The convergence of relative displacement error norm is shown in Fig.7 and the convergence of

relative energy error norm is shown in Fig.8. Fig.7 and Fig.8 show that the LMSLS leads to convergence results and the accuracy of the LMSLS method is better than the MLPG1 method. Compared with the results obtained using different size of nodal support in the LMSLS method, it can be found that a bigger-sized nodal support will impair the accuracy of the present method. On the contrary, the accuracy of the MLPG1 method is impaired substantially if a smaller-sized nodal support is used.
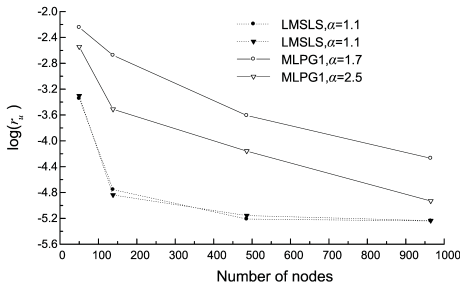
Figure 7: Convergence of relative displacement error norm
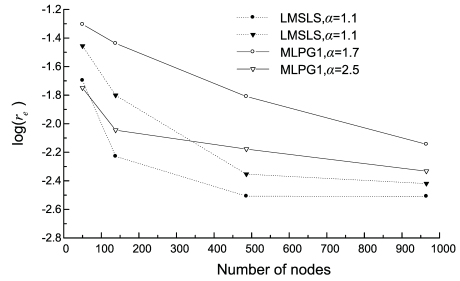
Figure 8: Convergence of relative energy error norm
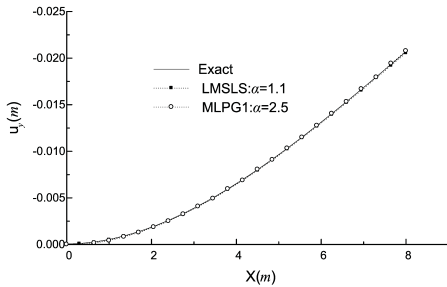
Figure 9: Deflection of the cantilever beam
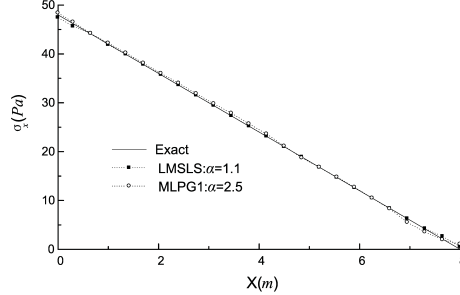
Figure 10: Normal stress of the cantilever beam

It is known that the MLS approximation is sensitive to the value of support radius d_{mi} which severely limits its usefulness [Belytschko, Lu and Gu (1994)]. However, the SLS interpolation alleviates this drawback and shows less sensitive to the radius d_{mi}. Furthermore, the reduction of the radius of nodal support means that fewer nodes are selected for the SLS interpolation than for the MLS approximation, and a lower computational cost is thus achieved.

The irregular distribution of 96 nodes employed here is shown in Fig.6(b). Fig.9 shows a comparison of the analytical solution, the MLPG1 solution and the present numerical solution for the beam deflection along x-axis. Fig.10 illustrates the com-

parison of normal stress σ_x at the section $y = d/2$. An excellent agreement with the analytical solution is observed in this problem.

As stated by Augarde and Deeks (2008), it should be noted that the exact solution in Eq. (36) is incorrect if boundary conditions are not matched exactly to the exact solution. However, the error in the solution is confined to the support region where the applied boundary condition does not match the analytical solution due to St Venant's effect, and thus the present LMSLS can still converge to the exact solution in Eq. (36).

Table 3: Comparison for Cook beam

Number of nodes	Methods	$\mathbf{V}_C$	σ_{Amax}	σ_{Bmin}
80	MLPG1	23.91	0.227	-0.206
	LMSLS	23.76	0.231	-0.201
206	MLPG1	24.41	0.236	-0.208
	LMSLS	24.33	0.235	-0.202
Reference solution		23.90	0.236	-0.201

4.4 Cook skew beam

A skew beam with distributed shear load $F = 1/16$ at the free edge is shown in Fig.11. The problem is modeled using 80 and 206 irregular nodes shown in Figure 12, and solved for plane stress case. The Young's modulus is 1 and Poission's ration is 1/3. $\alpha = 1.1$ is used in the LMSLS method and $\alpha = 1.7$ is used in the MLPG1 method. The deflection at point C, the maximum principal stress at point A and the minimum principal stress at point B are computed and listed in Tab.3 along with the results of reference solution [Chen, Cen, Long and Yao (2004)]. The quadratic basis function is used in this problem. It can be seen that the present LMSLS exhibits a good accuracy.

5 Conclusions

A Local Meshless Shepard and Least Square method (LMSLS) based on the local Petrov-Galerkin weak form is proposed for solving linear elasticity problems. The following are some of the important observations from the present work:

(1) The SLS interpolation employed in the LMSLS method possesses the Kronecker-delta property and thus the prescribed nodal displacement boundary conditions can be imposed as easily as in FEM.
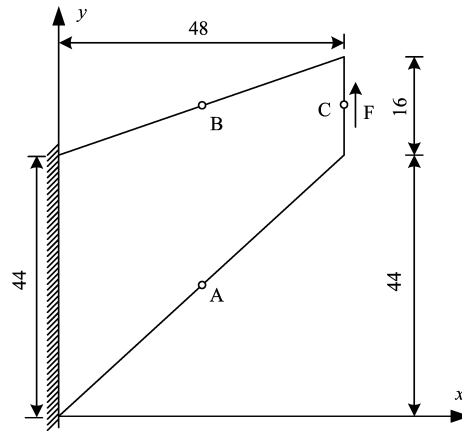
Figure 11: Cook skew beam

(a) 80 nodes   (b) 206 nodes
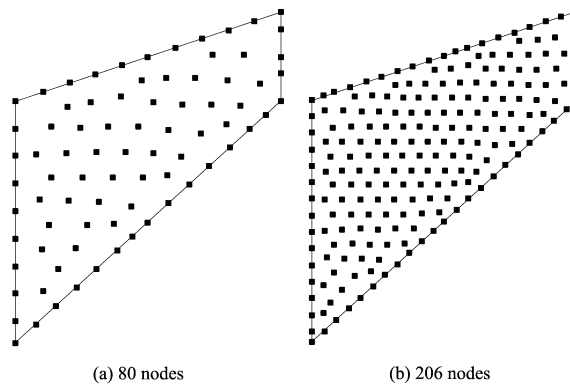
Figure 12: Nodal arrangements for Cook skew beam

(2) In contrast to other PU-based methods, the present SLS interpolation is truly meshless and has many merits, such as it requires no extra unknowns to define the local approximations of nodes and it avoids the problem of linear dependence.

(3) In the present LMSLS, the local polygons are constructed as integration domains, and three-node triangular FEM shape functions are chosen as the test functions. The new integration schedule, which can simplify the integration and the discrete equations of LMSLS, is truly meshless. It can be used in other MLPG type methods.

(4) Both the standard patch test and the constant strain patch test can be passed in LMSLS.

(5) In the present method, different sized nodal supports all lead to convergent results. However, increasing the radius of nodal support usually results in less accuracy. Numerical results indicate that the LMSLS method shows less sensitive to the value of nodal support radius than that of the MLPG1 method.

(6) The present LMSLS can be naturally extended to 3D problems. It is also beneficial in solving many problems such as progressive fracture and propagation interface because it is robust and mesh free.

References

Arefmanesh, A.; Najafi, M.; Abdi, H. (2008): Meshless local Petrov-Galerkin method with unity test function for non-isothermal fluid flow. *CMES: Computer Modeling in Engineering and Sciences*, vol.25, pp. 9-22.

Atluri, S. N.; Liu, H. T.; Han, Z. D. (2006a): Meshless Local Petrov-Galerkin (MLPG) mixed collocation method for elasticity problems. *CMES: Computer Modeling in Engineering and Sciences*, vol.14, pp. 141-152.

Atluri, S. N.; Liu, H. T.; Han, Z. D. (2006b): Meshless Local Petrov-Galerkin (MLPG) mixed finite difference method for solid mechanics. *CMES: Computer Modeling in Engineering and Sciences*, vol.15, pp. 1-16.

Atluri, S.N.; Zhu, T. (1998): A new Meshless Local Petrov-Galerkin (MLPG) approach in computational mechanics. *Computational Mechanics*, Vol.22, pp. 117-127.

Atluri, S. N.; Zhu, T. (2000): The Meshless Local Petrov-Galerkin(MLPG) approach for solving problems in elasto-statics. *Computational Mechanics*, vol. 25, pp. 169-179.

Atluri, S. N.; Shen, S. P. (2002): *The Meshless Local Petrov-Galerkin (MLPG) method*. Tech Science Press: Encino, CA, U.S.A.

Atluri, S. N.; Shen, S. P. (2005): Simulation of a 4(th) order ODE: Illustration of various primal & mixed MLPG methods, *CMES: Computer Modeling in Engineering and Sciences*, Vol. 7, pp. 241 - 268.

Augarde, C. E; Deeks, A. J. (2008): The use of Timoshenko's exact solution for a cantilever beam in adaptive analysis. *Finite Elements in Analysis and Design*, vol. 44, pp. 595-601.

Babuška, I.; Banerjee, U.; Osborn, J. E. (2004): Generalized ?nite element methods: main ideas results and perspectives. *International Journal of Computational Methods*, vol. 1, pp. 67-103.

Barry, W. (2004): A Wachspress meshless local Petrov-Galerkin method. *Engineering Analysis with Boundary Elements*, vol. 28, pp. 509-523.

Belytschko, T.; Lu, Y. Y.; Gu, L. (1994): Element-free Galerkin method. *International Journal for Numerical Methods in Engineering*, vol. 37, pp. 229-256.

Belytschko, T.; Krongauz, Y.; Organ, D. (1996): Meshless methods: An overview and recent developments. *Computer Methods in Applied Mechanics and Engineering*, vol. 139, pp. 3-47.

Cai, Y. C.; Zhu, H. H. (2004): A meshless local natural neighbour interpolation method for stress analysis of solids. *Engineering Analysis with Boundary Elements*, vol. 28, pp. 607-613.

Chen, S. S.; Liu, Y. H.; Cen, Z. Z. (2008): A combined approach of the MLPG method and nonlinear programming for lower-bound limit analysis. *CMES: Computer Modeling in Engineering and Sciences*, vol.28, pp. 39-55.

Chen, X. M.; Cen, S.; Long, Y. Q.; Yao, Z. H. (2004) Membrane elements insensitive to distortion using the quadrilateral area coordinate method. *Computers and Structures*, vol. 82, pp. 35-54.

Ching, H. K.; Chen, J. K. (2006): Thermomechanical analysis of functionally graded composites under laser heating by the MLPG method. *CMES: Computer Modeling in Engineering and Sciences*, vol.13, pp. 199-217.

Dang, T. D.; Sankar, B. V. (2008): Meshless local Petrov-Galerkin micromechanical analysis of periodic composites including shear loadings. *CMES: Computer Modeling in Engineering and Sciences*, vol.26, pp. 169-187.

Gao, L.; Liu, K.; Liu, Y. (2006): Applications of MLPG method in dynamic fracture problems. *CMES: Computer Modeling in Engineering and Sciences*, vol.12, pp. 181-195.

Gilhooley, D. F.; Xiao, J. R.; Batra, R. C. (2008): Two-dimensional stress analysis of functionally graded solids using the MLPG method with radial basis functions. *Computational Materials Science*, vol. 41, pp. 467-481.

Griebel, M.; Schweitzer, M. A. (2002): A particle-partition of unity method—Part II: efficient cover construction and reliable integration. *SIAM Journal on Scientific Computing*, vol. 23, pp. 1665–1682.

Gu Y. T.; Wang, Q. X.; Lam, K. Y. (2007): A meshless local Kriging method for large deformation analyses. *Computer Methods in Applied Mechanics and Engineering*, vol. 196, pp. 1673-1684.

Han, Z. D.; Atluri, S. N. (2004): Meshless Local Petrov–Galerkin (MLPG) approaches for solving 3D problems in elasto-statics. *CMES: Computer Modeling in Engineering and Sciences*, vol. 6, pp.169–188.

Han, Z. D.; Liu, H. T.; Rajendran, A. M.; Atluri, S. N. (2006): The applications of Meshless Local Petrov-Galerkin (MLPG) approaches in high-speed impact, penetration and perforation problems. *CMES: Computer Modeling in Engineering and Sciences*, vol.14, pp. 119-128.

Jarak, T.; Soric, J.; Hoster, J. (2007): Analysis of shell deformation responses by the Meshless Local Petrov-Galerkin (MLPG) approach. *CMES: Computer Modeling in Engineering and Sciences*, vol.18, pp. 235-246.

Krongauz Y., Belytschko T. (1997): Consistent pseudo-derivatives in meshless methods. *Computer Methods in Applied Mechanics and Engineering*, vol. 146, pp.371-386.

Lancaster, P.; Salkauskas, K. (1981): Surfaces generated by moving least squares methods. *Mathematics of Computation*, vol. 37, pp. 141-158.

Liu, G. R.; Gu, Y.T. (2001): A local point interpolation method for stress analysis of two-dimensional solids. *Structure Engineering and Mechanics*, vol. 2, pp. 221-236.

Li, S.; Atluri, S. N. (2008a): Topology-optimization of structures based on the MLPG mixed collocation method. *CMES: Computer Modeling in Engineering and Sciences*, vol.26, pp. 61-74.

Li, S.; Atluri, S. N. (2008b): The MLPG mixed collocation method for material orientation and topology optimization of anisotropic solids and structures. *CMES: Computer Modeling in Engineering and Sciences*, vol.30, pp. 37-56.

Long, S. Y.; Liu, K. Y.; Li, G. Y. (2008): An analysis for the elasto-plastic fracture problem by the meshless local Petrov-Galerkin method. *CMES: Computer Modeling in Engineering and Sciences*, vol.28, pp. 203-216.

Lu, Y. Y.; Belytschko, T. (1994): A new implementation of the element free Galerkin method. *Computer Methods in Applied Mechanics and Engineering*, vol. 113, pp. 397-414.

Macri, M.; De, S. (2008): An octree partition of unity method (OctPUM) with enrichments for multiscale modeling of heterogeneous media. *Computers and Structures*, vol. 86, pp.780–795.

Ma, Q. W. (2007): Numerical generation of freak waves using MLPG_R and

QALE-FEM methods. *CMES: Computer Modeling in Engineering and Sciences*, vol.18, pp. 223-234.

Ma, Q. W. (2008): A new meshless interpolation scheme for MLPG_R method. *CMES: Computer Modeling in Engineering and Sciences*, vol.23, pp. 75-89.

Melenk, J. M.; Babuška, I. (1996): The partition of unity finite element method: basic theory and applications. *Computer Methods in Applied Mechanics and Engineering*, vol.139, pp. 289-314.

Mohammadi, M. H. (2008): Stabilized Meshless Local Petrov-Galerkin (MLPG) method for incompressible viscous fluid flows. *CMES: Computer Modeling in Engineering and Sciences*, vol.29, pp. 75-94.

Oden, J. T.; Duarte, C. A.; Zienkiewicz, O. C. (1998): A new cloud-based hp finite element method. *Computer Methods in Applied Mechanics and Engineering*, vol. 153, pp. 117-126.

Oh, H. S.; Kimb, J. G.; Honga, W. T. (2008): The piecewise polynomial partition of unity functions for the generalized ?nite element methods. *Computer Methods in Applied Mechanics and Engineering*, doi:10.1016/j.cma. 2008.02.035

Pecher, R.; Elston, S.; Raynes, P. (2006): Meshfree solution of Q-tensor equations of nematostatics using the MLPG method. *CMES: Computer Modeling in Engineering and Sciences*, vol.13, pp. 91-101.

Rajendran, S.; Zhang, B. R. (2007): A"FE-meshfree" QUAD4 element based on partition of unity. *Computer Methods in Applied Mechanics and Engineering*, vol. 197, pp. 128-147.

Sladek, J.; Sladek, V.; Krivacek, J.; Wen, P. H.; Zhang, C. (2007): Meshless Local Petrov–Galerkin (MLPG) method for Reissner–Mindlin plates under dynamic load. *Computer Methods in Applied Mechanics and Engineering*, vol.196, pp. 2681-2691.

Sladek, J.; Sladek, V.; Solek, P.; Wen, P. H.; Atluri, S. N. (2008): Thermal analysis of Reissner-Mindlin shallow shells with FGM properties by the MLPG. *CMES: Computer Modeling in Engineering and Sciences*, vol.30, pp. 77-79.

Sladek, J.; Sladek, V.; Wen, P. H.; Aliabadi, M. H. (2006): Meshless Local Petrov-Galerkin (MLPG) method for shear deformable shells analysis. *CMES: Computer Modeling in Engineering and Sciences*, vol.13, pp. 103-117.

Sladek, J.; Sladek, V.; Zhang, C.; Solek, P. (2007): Application of the MLPG to thermo- piezoelectricity. *CMES: Computer Modeling in Engineering and Sciences*, vol.22, pp. 217-233.

Sladek, J.; Sladek, V.; Zhang, C.; Tan, C. L. (2006): Meshless local Petrov-Galerkin method for linear coupled thermoelastic analysis. *CMES: Computer Mod-*

eling in Engineering and Sciences, vol.16, pp. 57-68.

Timoshenko S. P.; Goodier J. N. (1970): *Theory of Elasticity*, McGraw-Hill, NewYork.

Vavourakis, V.; Sellountos, E. J.; Polyzos, D. (2006): A comparison study on different MLPG (LBIE) formulations. *CMES: Computer Modeling in Engineering and Sciences*, vol.13, pp. 171-183.

Yuan, W.; Chen, P.; Liu, K. (2007): A new quasi-unsymmetric sparse linear systems solver for Meshless Local Petrov-Galerkin method (MLPG). *CMES: Computer Modeling in Engineering and Sciences*, vol.17, pp. 115-134.